# Molecular Rotations and Dipole-Bound State Lifetimes

**David A. Walthall, Joel M. Karty,† and John I. Brauman***

*Department of Chemistry, Stanford University, Stanford, California 94305-5080*

*Received: January 3, 2005; In Final Form: July 21, 2005*

A computational model based on classical molecular rotation provides insight into the observability of dipole-bound states. The observability is related to the lifetime of the state prior to rotational autodetachment of the electron. The model tracks an ensemble of dipole-bound states. Their motion in space is integrated as a function of time, which provides a means to analyze the lifetimes of the dipole-bound states. The results are generally in good agreement with experimental data. Some exceptions show the limitations of the model but also provide insight into the autodetachment mechanism.

## Introduction

Dipole-bound states are nonvalence electronic states of anions that can be described semiclassically by the interaction between a distant electron and the dipole of a neutral core, Figure 1. These "exotic" electronic states have been shown to exist in several different anions, including the acetaldehyde enolate anion,[1−3] the cyanomethyl anion ($NCCH_2^-$),[4,5] and the water dimer complex anion ($(H_2O)_2^-$).[6] However, not all anions with substantial neutral core dipoles have observable dipole-bound states. Peculiarly, some of the anions that do not possess observable dipole-bound states are electronically very similar to others that do. For example, (*E*)-propen-1-olate, whose neutral core has a calculated dipole moment of 3.3 D, has observable dipole-bound states, whereas (*Z*)-propen-1-olate, whose neutral core has a calculated dipole moment of 3.0 D, does not (Figure 2).[7]

Dipole-bound states were first predicted in 1947 by Fermi and Teller in their paper investigating the capture of negative muons by hydrogen.[8] They noted that when the negatively charged muon approached the hydrogen atom it reached a critical distance, where the electron became unbound. They stated, without proof, that the critical distance was 0.639 $a_0$, which gives a critical dipole moment of 0.639 au. A derivation of this value was given in 1950 by Wightman.[9] These works were largely unnoticed, and subsequent work in the 1960s rederived this value.[10] Later work by Garrett showed that the critical dipole moment for real molecules is around 2 D.[11,12] In addition, he showed that the number of dipole-bound states is not infinite for real systems. The minimum dipole to support even two states is around 4.5 D.[13] This value depends on the length of the dipole moment and the moments of inertia.

Since the work of Fermi and Teller, there has been considerable work to characterize dipole-bound states. It is believed that the electron in a dipole-bound state occupies a very diffuse orbital, where the electron resides 50−200 Å away from the dipole of the neutral core.[5,14,15] As a result, the geometry of the neutral core is perturbed very little from that of the completely separated neutral and extra electron.[1,5,15,16] The binding energy of this electron is very weak, usually between 5 and 300 $cm^{-1}$.[1,5,15−17] Dipole-bound states of enolate anions have binding energies toward the low-energy end of this range.

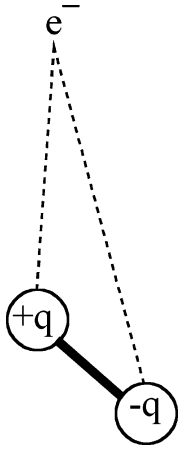


**Figure 1.** Classical representation of an electron interacting with a dipole.

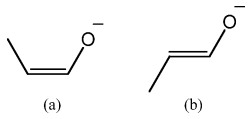


**Figure 2.** Enolate anions of propionaldehyde: (a) (*Z*)-propen-1-olate; (b) (*E*)-propen-1-olate.

There are two types of dipole-bound states that are now well established. In our experiments, a dipole-bound state is the excited state of an anion. Other experiments examine dipole-bound states that are ground states. These are formed by addition of an electron to a neutral species. This technique has been used to study a wide range of species.[18−23]

To observe dipole-bound states of anions, certain criteria must be met. First, the dipole-bound state must exist. Secondly, it must be possible to prepare the dipole-bound state species. In our experiments, anions are initially prepared in the ground electronic state so there must be a reasonably large optical cross section for the transition from the ground state of the anion to the excited electronic dipole-bound state (Figure 3). Finally, because dipole-bound states, in our experiments, are seen as sharp resonances near threshold, the dipole-bound state must autodetach and must do so in an appropriate time frame. It must

* Corresponding author. E-mail: brauman@stanford.edu.
† Current address: Department of Chemistry, Elon University, 2625 Campus Box, Elon, NC 27244.

10.1021/jp050025q CCC: $30.25 
Published on Web 09/08/2005

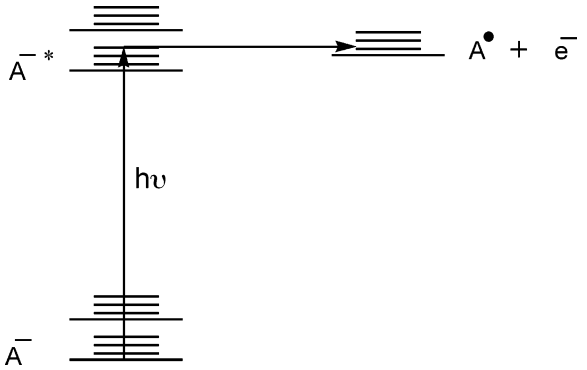


**Figure 3.** Photoexcitation to a dipole-bound state ($A^-$*) which autodetaches to the radical and a free electron.

autodetach faster than the trapping time of the anions but must also be long-lived enough to prevent excessive lifetime broadening.

In a previous paper, we presented the results of electron photodetachment spectroscopy of a series of alkylcyclohex-1-enolates and alkylcyclopent-1-enolates.[24] The species of the same ring size are all very similar electronically; they differ primarily in the placement of the alkyl group. However, their photodetachment spectra are quite different. Several of the species have observable dipole-bound states whereas others do not.

We believe that dipole-bound states exist for all enolates, including those studied in our previous paper, given that the calculated dipole moments (UHF/6-31+G*) of their neutral cores are all about 3−4 D. We also believe that the dipole-bound states in each of these species are reasonably accessible from the ground state. This is because all of the enolate species should have similar electronic-transition dipole moments from the ground state of the anion to the dipole-bound state. It is therefore likely that the difference between the enolate species that have observable dipole-bound states and those that do not lies in the third criterion for observability: those that do not have observable dipole-bound states are too short-lived, and the intensities of the otherwise observable resonances are below the noise of the background in the electron photodetachment spectra.

In the species where dipole-bound states are observable, there is considerable variation in the width of the dipole-bound state resonances. Most of the dipole-bound states that are created are so weakly bound that the lowest-energy resonance seen corresponds to a transition to the ground vibrational state.[3] Our resolution is too low to observe individual rotational lines, so we see the envelope of the P, Q, and R branches of the transition. In the absence of lifetime broadening effects, the rotational envelopes for electronically similar species should be roughly the same width.[25] The variation in width of observable dipole-bound states comes primarily from lifetime broadening. We believe that the species without observable dipole-bound states have dipole-bound states that are so lifetime broadened they arenot discernible above the background.

To explain these results, as well as related results of dipole-bound state observabilities that have previously been reported, we have developed a nearly classical computational model, based on molecular rotations, that provides insight into the lifetimes of dipole-bound states. This model tracks an ensemble of classical rotational trajectories of individual dipole-bound state anions to provide insight into their bulk observabilities. This is not the only possible source of lifetime broadening. For example, internal conversion could play a role. However, this model successfully predicts the behavior of a large number of molecules whose electronic structures are very similar, and it depends only on geometry.

Lykke, Neumark, Andersen, Trapa, and Lineberger studied the cyanomethyl anion and analyzed the dependence of the lifetime of the dipole-bound state as a function of the rotational state.[5] They found that the line width was nearly the same for all values of $J$ with constant $K$ up to $J = 32$. However, above this value, the line width increased rapidly as the lifetime decreased. They postulate that, above this value for $J$, the electron is not able to keep up with the motion of the dipole and lags behind. This causes the "catastrophic ejection" of the electron.

Our model provides a measure of the classical forces exerted by the moving dipole on the distant electron in each of several rotational states.[26] These forces provide a mechanism by which rotational energy can be transferred to the electron. This is important because, in a dipole-bound state, the electron is bound relative to the continuum (Figure 3), and for the electron to autodetach, there must be a transfer of energy from internal degrees of freedom to the electron. If a mechanism for energy transfer is available to a dipole-bound state in a given rotational state, it is conceivable that the lifetime of that dipole-bound state will be short. A dipole-bound state would not be expected to be observable under our experimental conditions if nearly all rotational states are too short lived. On the other hand, if there is a significant fraction of rotational states for which this mechanism is not in effect, the dipole-bound state is expected to be observable. We compute the fraction of trajectories for which the dipole of the neutral core remains inside a space-fixed cone of a given angle for a sufficiently long time. We observe that species which have experimentally observable dipole-bound states are generally those species that possess a significant fraction of these long-lived states.

## Computational Model

**Description.** A computational model was designed to provide insight into why dipole-bound state resonances are observed in the electron photodetachment spectra of some anions but not in others, even though the two species have similar electronic structures and dipole moments. We believe that the difference lies in the lifetime of the dipole-bound state, and the mechanism for autodetachment is rotational to electronic coupling. Our model concentrates on the lowest-energy dipole-bound state resonance, which is the ground vibrational state.

Because the loosely bound electron in a dipole-bound state is bound by charge−dipole interactions, the most favorable position for an electron is along the dipole at the positive end. Our model places the electron in this most favorable position. The species is given an angular momentum vector with a random length and orientation. An ensemble of these species has an isotropic distribution of angular momenta, so each one is weighted to make the distribution physically realistic. The electron is frozen in space, and the neutral core is allowed to rotate freely according to the physical constraints on that species. We feel that it is reasonable to freeze the electron because it is very far away from the core, which requires the electron to move much faster than the core. In addition, it has previously been seen that the electron can fail to keep up with the rotating core.[5]

At any given time, the dipole moment can be decomposed into two components, one parallel to the electron−core line and one perpendicular to it. When the parallel component of the dipole moment drops below the critical dipole length, $\mu_{crit}$, the electron is considered unbound.

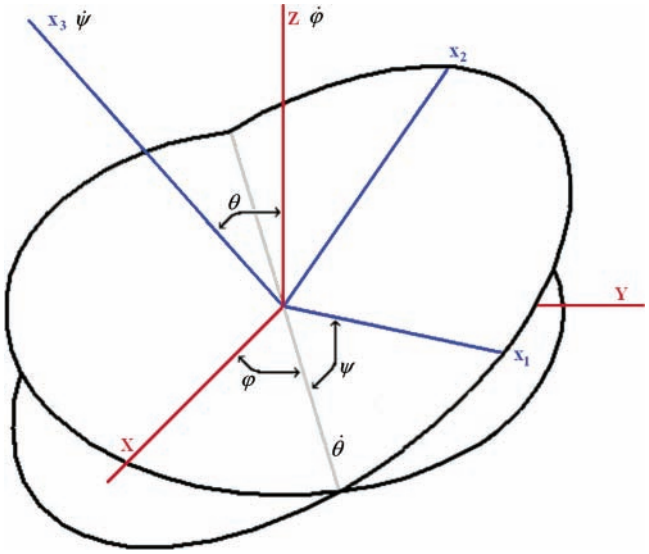


**Figure 4.** Diagram showing the relationship between the space-fixed axes ($X$, $Y$, and $Z$) and the molecular-fixed principal axes ($x_1$, $x_2$, and $x_3$) through the Euler angles ($\theta$, $\varphi$, and $\psi$). The principal axes are sometimes denoted $A$, $B$, and $C$, instead of $x_1$, $x_2$, and $x_3$.

This simplistic approach attempts to model the rotational−electronic coupling by looking at the forces on the electron. The model makes several assumptions. First, it is assumed that the geometry of the neutral core is the same as the geometry of the radical. This is reasonable, given that the extra electron is very far from the core and that the geometries of the anion and the radical are very similar. Secondly, the neutral core is treated as a rigid rotor. In particular, no internal motions are allowed during the simulation. Thirdly, the electron is considered to be frozen in space. In reality, the electron would move to maintain its favorable position behind the positive end of the dipole. For slow motions of the dipole, this would be possible, but for fast motions of the dipole, the electron would be unable to keep up and would autodetach. Because of the physical manner in which rigid objects rotate, slow motions of the dipole generally mean that the dipole never moves very far from its initial position and fast motions generally mean that the dipole's position changes drastically in space. In addition, even if the dipole is moving very fast over a small angular displacement, there is very little force on the electron. It is therefore reasonable to make the electron frozen in space because this approximates the forces on the electron. Finally, it is assumed that the electron exerts no forces on the core and does not affect the motion of the core. The effect of the electron should be relatively small because the distance between the electron and the core is so large.

**Details.** Modeling of the rotational motion of the neutral core requires the differential equations of motion of the neutral core in the lab-fixed frame, as well as the three principal moments of inertia ($I_1$, $I_2$, and $I_3$) and the dipole moment. The moments of inertia and the dipole moment of the neutral core are assumed to be the same as those for the radical. They were calculated at the UHF/6-31+G* level of theory using Gaussian 98.[27] The relationship between the principal axes in the body-fixed frame ($x_1$, $x_2$, and $x_3$) and the axes in the lab-fixed frame ($X$, $Y$, and $Z$) are given by Euler angles ($\theta$, $\varphi$, and $\psi$), as shown in Figure 4.

To obtain the differential equations of motion of the neutral core in the lab-fixed frame, we must know the time dependence of the Euler angles. To do this, we follow the procedure that is used by many classical mechanics books on the treatment of the rotation of rigid bodies.[28−30] We first obtain the angular velocities along the principal axes. By projecting the time derivatives of the Euler angles, shown in Figure 4, onto the principal axes and collecting the terms, we obtain eq 1,

$$\begin{aligned}\Omega_1 &= \mathrm{d}\varphi/\mathrm{d}t \sin\theta \sin\psi + \mathrm{d}\theta/\mathrm{d}t \cos\psi \\ \Omega_2 &= \mathrm{d}\varphi/\mathrm{d}t \sin\theta \cos\psi - \mathrm{d}\theta/\mathrm{d}t \sin\psi \\ \Omega_3 &= \mathrm{d}\varphi/\mathrm{d}t \cos\theta + \mathrm{d}\psi/\mathrm{d}t \end{aligned} \quad (1)$$

where $\Omega$ is the angular velocity and $\Omega_i$ is the angular velocity along the principal axis $x_i$. Because the initial choice of the lab-fixed frame is completely arbitrary, we choose it so that **M**, the angular momentum, is along $Z$. We now decompose the angular momentum into its values along each of the principal axes, as shown in eq 2

$$\begin{aligned}M_1 &= M \sin\theta \sin\psi \\ M_2 &= M \sin\theta \cos\psi \\ M_3 &= M \cos\theta \end{aligned} \quad (2)$$

where $M = |\mathbf{M}|$. Finally, because $x_1$, $x_2$, and $x_3$ are the principal axes of the molecule, $M_i = I_i\Omega_i$. Combining this with eqs 1 and 2, we obtain a system of 3 simultaneous equations for $\mathrm{d}\theta/\mathrm{d}t$, $\mathrm{d}\varphi/\mathrm{d}t$, and $\mathrm{d}\psi/\mathrm{d}t$ in terms of $\theta$, $\psi$, $M$, $I_1$, $I_2$, and $I_3$. Solving this system of equations gives the time derivatives of the Euler angles, as shown in eq 3.

$$\begin{aligned}\mathrm{d}\theta/\mathrm{d}t &= \frac{M(I_2 - I_1)}{I_1 I_2}\sin\theta \cos\psi \sin\psi \\ \mathrm{d}\varphi/\mathrm{d}t &= \frac{M}{I_1 I_2}[I_2 + (I_1 - I_2)\cos^2\psi] \\ \mathrm{d}\psi/\mathrm{d}t &= \left[\frac{M}{I_3} - \mathrm{d}\varphi/\mathrm{d}t\right]\cos\theta \end{aligned} \quad (3)$$

As a measure of the forces exerted by the dipole on the distant electron in a given rotational trajectory, we compute the time required for the projection of the moving dipole onto the original dipole position to be less than the critical dipole moment of 1.625 D. This forms a cone around the initial dipole position in the lab-fixed frame. Less time to leave this cone means that the electron becomes unbound more quickly. To determine this "residence time" of the dipole inside the cone, we numerically integrated the differential equations of motion of the molecule in the lab-fixed frame (eq 3) over time, using the fourth-order Runge−Kutta method with a time step of 5 au (roughly $1.2 \times 10^{-16}$ s).[31] After each step, the projection of the dipole onto its position at time zero was calculated.

For each species, the fraction of rotational trajectories with the dipole remaining inside the space-fixed cone was plotted as a function of time. This determined the fraction of trajectories for which the dipole has a long residence time inside the cone, i.e., for which the electron is bound during the entire simulation. At least $10^5$ rotational trajectories were run on each species studied. For each trajectory, the dipole's residence time inside the cone and relative abundance were recorded. Each trajectory was assigned to a bin, $6 \times 10^{-14}$ s wide, according to the dipole's computed residence time inside the cone. Once a trajectory was assigned to a bin, its relative abundance ($N_i$) was added into the appropriate bin. When all of the rotational trajectories had been run for a given species, each bin represented the fraction of rotational trajectories that exited the cone in that time slice. The fraction of trajectories with the dipole

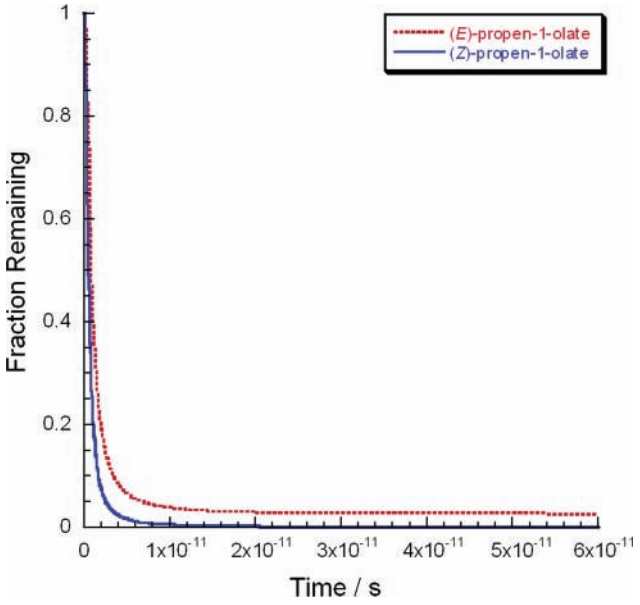


**Figure 5.** Computed decay curve of (*E*)-propen-1-olate and (*Z*)-propen-1-olate.

remaining inside the cone as a function of time was computed from this set of data. We define the plot of the fraction of trajectories for which the dipole is inside the cone vs time as the species' decay curve.

The relative abundance, $N_i$, of each of these randomly chosen trajectories in a thermalized ensemble was then calculated. Each trajectory was weighted according to its rotational energy and its quantum mechanical degeneracy, $(2M + 1)$, according to eq 4 where $M$ is the magnitude of the angular momentum, $E_{rot}$ is

$$N_i = (2M + 1) \exp(-E_{rot}/kT) \quad (4)$$

the rotational energy of the given rotational state, $k$ is the Boltzmann constant, and $T$ is the temperature in Kelvin, taken to be that measured in the ICR cell (350 K).[32] The normalization factor, $N_{tot}$, is given in eq 5 where the sum is over all rotational trajectories computed.

$$N_{tot} = \sum_{i=1}^{10^5} N_i \quad (5)$$

## Results

Figure 5 shows the decay curve for (*E*)-propen-1-olate and (*Z*)-propen-1-olate. For (*E*)-propen-1-olate, the falloff region decays asymptotically to a nonzero fraction, whereas for (*Z*)-propen-1-olate, the curve decays asymptotically to zero. The value of the asymptote is taken to be the fraction of trajectories for which the dipole has a long residence time within the cone. Table 1 summarizes the results from decay curves of the species studied in a previous paper,[24] as well as some other anions that have been studied.

## Discussion

Several other models have addressed dipole-bound state lifetimes. A rotationally adiabatic model was developed by Clary,[14] and later modified by Simons,[37] to describe the autodetachment dynamics of electrons in dipole-bound states. That model involves diagonalizing a Hamiltonian that consists of a repulsive core, an electron−dipole interaction term, and a damped polarization term. The rotationally adiabatic model and its modification are semiclassical models that provide insight into the lifetimes of dipole-bound states in individual rotational states.

**TABLE 1: Computational Model Results and Dipole-Bound State Observability**

| anion species | observed dipole-bound state resonances[a] | fraction of trajectories with long residence times (%) |
|---|---|---|
| cyclobut-1-enolate[b] | narrow | 7 |
| cyclopent-1-enolate[b] | narrow | 8 |
| 2-methylcyclopent-1-enolate[c] | none | ∼0 |
| 3-methylcyclopent-1-enolate[c] | narrow, as a mixture | 3 |
| 4-methylcyclopent-1-enolate[c] | narrow, as a mixture | 3 |
| 5-methylcyclopent-1-enolate[c] | none | ∼0 |
| cyclohex-1-enolate[b] | narrow | 9 |
| 2-methylcyclohex-1-enolate[c] | none | ∼0 |
| 3-methylcyclohex-1-enolate[c] | none, as a mixture | 1 |
| 4-methylcyclohex-1-enolate[c] | narrow | 7 |
| 4-ethylcyclohex-1-enolate[c] | none | 5 |
| 5-methylcyclohex-1-enolate[c] | none, as a mixture | ∼0 |
| 6-methylcyclohex-1-enolate[c] | broad | ∼0 |
| cyclohept-1-enolate[b] | none | 8 |
| $\beta$-propiolactone enolate[d] | narrow | 3 |
| $\gamma$-butyrolactone enolate[d] | narrow | 6 |
| $\delta$-valerolactone enolate[d] | narrow | 8 |
| $\epsilon$-caprolactone enolate[d] | none | 9 |
| acetaldehyde enolate[e] | narrow | 2 |
| acetone enolate[f] | broad | ∼0 |
| pinacolone enolate[b] | none | ∼0 |
| acetyl fluoride enolate[g] | narrow | ∼0 |
| (*E*)-propen-1-olate[h] | narrow | 3 |
| (*Z*)-propen-1-olate[h] | none | ∼0 |
| cyanomethyl[i] | narrow | 3 |

[a] For species reported "as mixture", the photodetachment spectrum was taken as a mixture with another species. It is unclear which species the dipole-bound state resonance belongs to, although they are similar enough that we believe that they would either both have observable dipole-bound resonances or both not have them. [b] Reference 33. [c] Reference 24. [d] Reference 34. [e] References 1−3 and 35. [f] References 33 and 36. [g] Reference 16. [h] Reference 7. [i] References 4, 5, and 25.

For the cyanomethyl anion and the enolate anion of acetaldehyde, dipole-bound state lifetimes of individual rotational states calculated from the rotationally adiabatic model are in relatively good agreement with those measured by Lineberger and co-workers.[1,5] Despite these successes, it is difficult to use the rotationally adiabatic model to understand the observability of dipole-bound state resonances in electron photodetachment spectroscopy. The rotationally adiabatic model provides information about individual rotational states but is very complex. In contrast, our model only provides information about the overall observability of the rotational envelope of the dipole-bound state. For rotationally resolved data, the rotationally adiabatic model is more appropriate. However, our model appears to be sufficient to explain our experiments and easier to use for more complex molecules.

Brinkman et al. proposed that the envelope of rotational states of a dipole-bound state should be observable if the lifetimes of the individual rotational states are long enough.[33] They further suggested that the lifetimes of rotational states depend on the motion of the dipole. If, in a particular rotational state of the molecule, the dipole does not have significant motion, then the lifetime will be long. On the other hand, if the dipole tumbles in space, then the lifetime will be short. In that model, the molecule is assumed to be a near-symmetric top and the motion of the dipole is dependent only on the angle between the dipole moment vector and the figure axis (the axis of symmetry). In the symmetric top limit, the angular momentum vector, **M**,

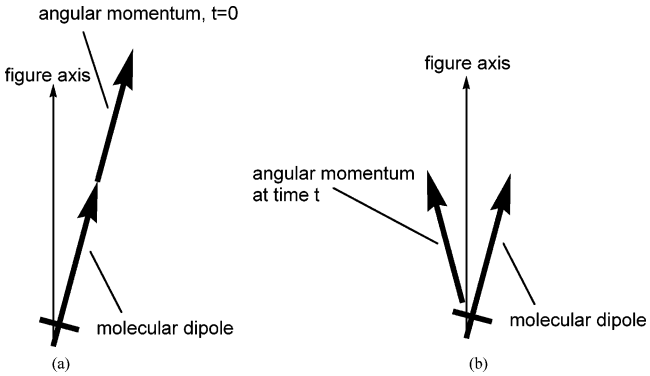


**Figure 6.** Example in which the angle between the figure axis and the dipole is small. (a) Molecular rotation about the dipolar axis that initially leaves the dipole fixed in space. (b) Precession of the angular momentum vector about the $x_1$ axis eventually leads to motion of the dipole.

precesses around the figure axis for **M** close to that axis. If the angle between the dipole moment and the figure axis is too large, there will be no rotations that leave the dipole fixed in space (Figure 6a,b). Because **M** is fixed in space, motion of **M** in the body-fixed frame corresponds to motion of the molecule in the lab-fixed frame.

Brinkman's model assumed that all of the species were near-symmetric tops. For molecules that could not be approximated as symmetric tops, it was suggested that the dipole would always rotate in space and, consequently, the dipole-bound state would have a very short lifetime.

That model was reasonably successful in explaining the observability of dipole-bound states. However, that model is incomplete for two reasons. Most enolate anions that have been studied, both those that have observable dipole-bound states and those that do not, are far from symmetric tops. Although the model makes the argument that asymmetric tops should show no dipole-bound states, the enolate anions of cyclohexanone, cyclopentanone, and cyclobutanone are asymmetric tops that have observable dipole-bound states. In addition, it has long been known that the motion of an asymmetric top can be coherent if the angular momentum is near $x_1$ or $x_3$.[28]

The model that we have developed here was designed to track classical rotational trajectories of neutral cores of dipole-bound state anions to provide information about the forces exerted on the distant electron by the moving dipole. These forces provide a mechanism by which energy can be transferred from molecular rotation to the electron; large forces can conceivably decrease the lifetime of the dipole-bound state and preclude it from being observable. To understand the extent of these forces in an ensemble of rotational trajectories of a given species, we computed, as a function of time, the fraction of trajectories for which the projection of the dipole onto the original dipole exceeds the critical dipole value of 1.625 D. The results of these decay curves are summarized in Table 1.

**Correlation Between Decay Curves and Dipole-Bound State Observability.** There appears to be a good correlation between the observability of the dipole-bound state in a given species and the fraction of trajectories with a long residence time inside the space-fixed cone, determined from its decay curve (Table 1). That is, a species that has a significant nonzero fraction of trajectories with a long residence time of the dipole inside the cone has an electron photodetachment spectrum in which narrow dipole-bound state resonances ($\leq$5 nm full width at half-maximum) are observable. Conversely, those species that have no trajectories for which the dipole has a long residence time inside the cone do not have electron photodetachment spectra in which narrow resonances are observable; either the resonances do not appear in the spectrum, or, in the case of 6-methylcyclohex-1-enolate and the enolate anion of acetone, the resonance is significantly broadened.

All of the species listed in Table 1 are consistent with this correlation, with the exceptions of the enolate anions of acetyl fluoride, cycloheptanone, and $\epsilon$-caprolactone. The enolate anion of acetyl fluoride has no trajectories predicted in its decay curve for which the dipole has a long residence time, but its electron photodetachment spectrum possesses narrow dipole-bound state resonances. The enolate anions of cycloheptanone and $\epsilon$-caprolactone, on the other hand, have a significant fraction of trajectories in which the dipole has a long residence time inside the cone, but no dipole-bound state resonances appear in their electron photodetachment spectra.

We believe that the enolate anion of acetyl fluoride is an exception because the electron in its dipole-bound state is more strongly bound (35 $cm^{-1}$)[16] than other enolate anions in the table, such as the enolate anion of acetaldehyde (5 $cm^{-1}$).[1] As a consequence, for similar rotational trajectories, the electron in the dipole-bound state of the acetyl fluoride enolate anion is more able to keep up with the rotating dipole than the extra electron in the dipole-bound state of the acetaldehyde enolate anion. Because acetyl fluoride is so strongly bound, the same forces that would autodetach a less strongly bound anion are insufficient to autodetach acetyl fluoride. This hypothesis is supported by results from photodetachment spectroscopy.[16] In the photodetachment spectrum of the enolate anion of acetaldehyde, the maximum angular momentum quantum number, $N$, for which the dipole-bound state is observable is $N = 7$, whereas the dipole-bound state of the enolate anion of acetyl fluoride is observable for $N$ as large as 20.

A second class of exceptions is the enolate anions of the seven-membered rings. We believe that this results from the "floppiness" of the rings. Strong coupling between the low-energy vibrational modes of the ring and the overall molecular rotation of the species is not accounted for in the computational model, which assumes that the molecule is rigid. This hypothesis is supported by other research, which has shown that rings with an odd number of rings are floppy.[38−40] Even if the vibrationless seven-membered ring enolate anions have a significant fraction of trajectories for which the dipole has a long residence time, as predicted by our model, the vibration−rotation coupling serves to disrupt the coherence of those stable trajectories. Consequently, the seven-membered ring enolate anions effectively have no trajectories for which the dipole has a long residence time.

Additional support for the strong vibration−rotation coupling in the seven-membered rings comes from the fact that, in both the series of cyclic ketone enolate anions and the series of lactone (cyclic ester) enolate anions, dipole-bound states are experimentally observable in the four, five, and six-membered rings, for which the rings are more rigid, but not in the seven-membered rings.

Although our model is well-suited to the study of the excited dipole-bound states seen in our experiments, it does not appear to be applicable to the study of the ground-state dipole supported anions seen in other studies.[18−23] The anions in those experiments are generated from neutrals that are rotationally and vibrationally cooled in a supersonic expansion. Compton notes that this cooling is important for the production of these anions, especially those with small dipole moments.[22] The dipole-bound states formed from excitation of enolates are bound fairly

weakly, about 5 $cm^{-1}$, and the ground-state dipole-bound anions are bound more strongly, 10−70 $cm^{-1}$, depending on the species studied. On the basis of our results for acetyl fluoride, we expect this model to not be applicable to these ground-state dipole-bound anion systems.

## Summary

We have developed a nearly classical model to predict the observability of dipole-bound states. In the model, the neutral core of the dipole-bound state is approximated as a rigid rotor and is allowed to rotate freely. This affects the binding of the extra electron, which is frozen in space. The model is successful in explaining the observability of dipole-bound states, although there are a few exceptions. These exceptions are analyzed and can provide insight into their mode of autodetachment.

**Acknowledgment.** We thank the National Science Foundation for support of this research. D.W. is grateful to Atofina for a graduate fellowship.

## References and Notes

(1) Mead, R. D.; Lykke, K. R.; Lineberger, W. C.; Marks, J.; Brauman, J. I. *J. Chem. Phys.* **1984**, *81*, 4883−4892.
(2) Lykke, K. R.; Mead, R. D.; Lineberger, W. C. *Phys. Rev. Lett.* **1984**, *52*, 2221−2224.
(3) Jackson, R. L.; Hiberty, P. C.; Brauman, J. I. *J. Chem. Phys.* **1981**, *74*, 3705−3712.
(4) Marks, J.; Wetzel, D. M.; Comita, P. B.; Brauman, J. I. *J. Chem. Phys.* **1986**, *84*, 5284−5289.
(5) Lykke, K. R.; Neumark, D. M.; Andersen, T.; Trapa, V. J.; Lineberger, W. C. *J. Chem. Phys.* **1987**, *87*, 6842−6853.
(6) Hendricks, J. H.; De Clercq, H. L.; Lyapustina, S. A.; Fancher, C. A.; Lippa, T. P.; Collins, J. M.; Arnold, S. T.; Lee, G. H.; Bowen, K. H. *Front. Sci. Ser.* **1996**, *16*, 321−328.
(7) Römer, B.; Brauman, J. I. *J. Am. Chem. Soc.* **1997**, *119*, 2054−2055.
(8) Fermi, E.; Teller, E. *Phys. Rev.* **1947**, *72*, 399−408.
(9) Wightman, A. S. *Phys. Rev.* **1950**, *77*, 521−528.
(10) Turner, J. E. *Am. J. Phys.* **1977**, *45*, 758−766.
(11) Garrett, W. R. *Bull. Am. Phys. Soc.* **1970**, *15*, 1336.
(12) Garrett, W. R. *Chem. Phys. Lett.* **1970**, *5*, 393−397.
(13) Garrett, W. R. *J. Chem. Phys.* **1980**, *73*, 5721−5725.
(14) Clary, D. C. *J. Phys. Chem.* **1988**, *92*, 3173−3181.
(15) Gutowski, M.; Skurski, P. *Recent Res. Dev. Phys. Chem.* **1999**, *3*, 245.
(16) Marks, J.; Brauman, J. I.; Mead, R. D.; Lykke, K. R.; Lineberger, W. C. *J. Chem. Phys.* **1988**, *88*, 6785−6792.
(17) Yokoyama, K.; Leach, G. W.; Kim, J. B.; Lineberger, W. C.; Boldyrev, A. I.; Gutowski, M. *J. Chem. Phys.* **1996**, *105*, 10706−10718.
(18) Carles, S.; Desfrançois, C.; Schermann, J. P.; Jalbout, A. F.; Adamowicz, L. *Chem. Phys. Lett.* **2001**, *334*, 374−380.
(19) Desfrançois, C.; Baillon, B.; Schermann, J. P.; Arnold, S. T.; Hendricks, J. H.; Bowen, K. H. *Phys. Rev. Lett.* **1994**, *1*, 48−51.
(20) Desfrançois, C.; Periquet, V.; Bouteiller, Y.; Schermann, J. P. *J. Phys. Chem. A* **1998**, *102*, 1274−1278.
(21) Desfrançois, C.; Periquet, V.; Lyapustina, S. A.; Lippa, T. P.; Robinson, D. W.; Bowen, K. H.; Nonaka, H.; Compton, R. N. *J. Chem. Phys.* **1999**, *111*, 4569−4576.
(22) Hammer, N. I.; Diri, K.; Jordan, K. D.; Desfrançois, C.; Compton, R. N. *J. Chem. Phys.* **2003**, *119*, 3650−3660.
(23) Hammer, N. I.; Hinde, R. J.; Compton, R. N.; Diri, K.; Jordan, K. D.; Radisic, D.; Stokes, S. T.; Bowen, K. H. *J. Chem. Phys.* **2004**, *120*, 685−690.
(24) Walthall, D. A.; Karty, J. M.; Römer, B.; Ursini, O.; Brauman, J. I. *J. Phys. Chem. A* **2005**, *109*, 8785−8793.
(25) Wetzel, D. M.; Brauman, J. I. *J. Chem. Phys.* **1989**, *90*, 68−73.
(26) Classically, an electron a fixed distance from the center of a dipole is lowest in energy in the configuration, with the electron along the dipolar axis at the positive end. If the dipole tips off axis and the electron fails to keep up, there will be a force exerted on the electron in the direction of the motion of the positive end.
(27) Frisch, M. J.; Trucks, G. W.; Schlegel, H. B.; Scuseria, G. E.; Robb, M. A.; Cheeseman, J. R.; Zakrzewski, V. G.; Montgomery, J. A., Jr.; Stratmann, R. E.; Burant, J. C.; Dapprich, S.; Millam, J. M.; Daniels, A. D.; Kudin, K. N.; Strain, M. C.; Farkas, O.; Tomasi, J.; Barone, V.; Cossi, M.; Cammi, R.; Mennucci, B.; Pomelli, C.; Adamo, C.; Clifford, S.; Ochterski, J.; Petersson, G. A.; Ayala, P. Y.; Cui, Q.; Morokuma, K.; Malick, D. K.; Rabuck, A. D.; Raghavachari, K.; Foresman, J. B.; Cioslowski, J.; Ortiz, J. V.; Baboul, A. G.; Stefanov, B. B.; Liu, G.; Liashenko, A.; Piskorz, P.; Komaromi, I.; Gomperts, R.; Martin, R. L.; Fox, D. J.; Keith, T.; Al-Laham, M. A.; Peng, C. Y.; Nanayakkara, A.; Challacombe, M.; Gill, P. M. W.; Johnson, B.; Chen, W.; Wong, M. W.; Andres, J. L.; Gonzalez, C.; Head-Gordon, M.; Replogle, E. S.; Pople, J. A. *Gaussian 98*, revision A.9; Gaussian, Inc.: Pittsburgh, PA, 1998.
(28) Landau, L. D.; Liftshitz, E. M. *Mechanics*; Pergamon Press: New York, 1960; Vol. 1.
(29) Yeh, H.; Abrams, J. I. *Principles of Mechanics of Solids and Fluids. Particle and Rigid-Body Mechanics*, 1st ed.; McGraw-Hill Book Company, Inc.: York, PA, 1960; Vol. 1.
(30) Goldstein, H. *Classical Mechanics*; Addison-Wesley Publishing Company, Inc.: Reading, MA, 1980.
(31) Although the Runge−Kutta integration algorithm was accurate using much larger time steps, we limited the time step to 5 au to obtain better accuracy of the trajectory lifetimes.
(32) Han, C. C.; Brauman, J. I. *J. Am. Chem. Soc.* **1989**, *111*, 6491−6496.
(33) Brinkman, E. A.; Berger, S.; Marks, J.; Brauman, J. I. *J. Chem. Phys.* **1993**, *99*, 7586−7594.
(34) Karty, J. M.; Janaway, G. A.; Brauman, J. I. *J. Am. Chem. Soc.* **2002**, *124*, 5213−5221.
(35) Mullin, A. S.; Murray, K. K.; Schulz, C. P.; Szaflarski, D. M.; Lineberger, W. C. *Chem. Phys.* **1992**, *166*, 207−213.
(36) Ellison, G. B.; Engelking, P. C.; Lineberger, W. C. *J. Phys. Chem.* **1982**, *86*, 4873−4878.
(37) Simons, J. *J. Chem. Phys.* **1989**, *91*, 6858−6865.
(38) Dale, J. *Acta Chem. Scand.* **1973**, *27*, 1130−1148.
(39) Anet, F. A. L.; St. Jacques, M.; Henrichs, P. M.; Cheng, A. K.; Krane, J.; Wong, L. *Tetrahedron* **1974**, *30*, 1629−1637.
(40) Still, W. C.; Galynker, I. *Tetrahedron* **1981**, *37*, 3981−3996.